Biogeosciences Discuss., doi:10.5194/bg-2015-606, 2016
Manuscript under review for journal Biogeosciences
Published: 2 February 2016

Biogeosciences Discussions
Open Access
EGU

Shifts in the microbial community in the Baltic Sea with increasing CO_2

K. J. Crawfurd[1], U. Riebesell[2], and C. P. D. Brussaard[1,3]

[1]Department of Biological Oceanography, NIOZ – Royal Netherlands Institute for Sea Research, P.O. Box 59, 1790 AB Den Burg, Texel, the Netherlands
[2]GEOMAR Helmholtz Centre for Ocean Research Kiel, Kiel, Germany
[3]Aquatic Microbiology, Institute for Biodiversity and Ecosystem Dynamics, University of Amsterdam, P.O. Box 94248, 1090 GE Amsterdam, the Netherlands

Received: 28 November 2015 – Accepted: 6 December 2015 – Published: 2 February 2016

Correspondence to: K. J. Crawfurd (kate.crawfurd@nioz.nl)

Published by Copernicus Publications on behalf of the European Geosciences Union.

Abstract

Ocean acidification, due to dissolution of anthropogenically produced carbon dioxide is considered a major threat to marine ecosystems. The Baltic Sea, with extremely low salinity and thus low pH buffering capacity, is likely to experience stronger variation in pH than the open ocean with increasing atmospheric carbon dioxide. We examined the effects of ocean acidification on the microbial community during summer using large volume in situ mesocosms to simulate present to future and far future scenarios. We saw distinct trends with increasing CO_2 in each of the 6 groups of phytoplankton with diameters below 20 µm that we enumerated by flow cytometry. Of these groups two picoeukaryotic groups increased in abundance whilst the other groups, including prokaryotic *Synechococcus* spp., decreased with increasing CO_2. Gross growth rates increased with increasing CO_2 in the dominant picoeukaryote group sufficient to double their abundances whilst reduced grazing allowed the other picoeukaryotes to flourish at higher CO_2. Significant increases in lysis rates were seen at higher CO_2 in these two picoeukaryote groups. Converting abundances to particulate organic carbon we saw a large shift in the partitioning of carbon between the size fractions which lasted throughout the experiment. The heterotrophic prokaryotes largely followed the algal biomass with responses to increasing CO_2 reflecting the altered phytoplankton community dynamics. Similarly, higher viral abundances at higher CO_2 seemed related to increased prokaryote biomass. Viral lysis and grazing were equally important controlling prokaryotic abundances. Overall our results point to a shift towards a more regenerative system with potentially increased productivity but reduced carbon export.

1 Introduction

Ocean acidification (OA) caused by anthropogenic carbon dioxide (CO_2) release and its subsequent dissolution in the oceans is considered one of the great threats facing marine ecosystems (Turley and Boot, 2010). Direct and indirect effects are predicted to

BGD

doi:10.5194/bg-2015-606

have a large impact on many marine ecosystems including phytoplankton communities which have the potential to alter global biogeochemistry (IPCC, 2007). This study was performed in the Gulf of Finland in the Baltic sea near Tvärminne, which is brackish with salinity 5.7–6.6 due to high amounts of freshwater runoff (Merkouriadi and Leppäranta, 2014). Brackish waters have a low pH buffering capacity due to low total alkalinity, related to the low salinity. Thus temporal pH variability will be greater due to the greater effects of biological processes ie. photosynthesis and respiration and non-biological factors driving pH change in association with the low buffering capacity (Dickinson et al., 2013; Jansson et al., 2013).

Marine phytoplankton are responsible for approximately half of global primary production (Field et al., 1998), shelf sea communities contribute 15–30 % of this and as much as 80 % of organic matter burial (Kulinski and Pempkowiak, 2011). Phytoplankton community production and composition have been found to be susceptible to effects of OA (Tortell et al., 2002; Engel et al., 2007; Feng et al., 2009; Meakin and Wyman, 2011). Diatoms, important for organic matter burial, have been found to benefit in some cases (Feng et al., 2009) but not in others (Tortell et al., 2002). Calcification of coccolithophores, which influence sedimentation via calcium carbonate ballasting, is generally reduced (Meyer and Riebesell, 2015). Pico-eukaryotes, responsible for > 40 % of primary production in some oceanic regions (Grob et al., 2011) and certain cyanobacteria, including diazatrophs, have been seen to benefit from elevated CO_2 (Barcelos e Ramos et al., 2007; Engel et al., 2007; Hutchins, 2007; Meakin and Wyman, 2011; Qiu and Gao, 2002). Phytoplankton growth and carbon fixation (Hein and Sand-Jensen, 1997), organic matter production (Leonardos and Geider, 2005; Zondervan et al., 2002) and extracellular organic matter production (Engel, 2002) may also be enhanced by more available CO_2, depending on the phytoplankton community composition.

Production is, however, balanced by losses, so whilst environmental factors regulate gross primary production bottom-up, factors such as grazing, viral lysis and sedimentation determine the fate of the carbon fixed by phytoplankton. Ingested carbon transfers to higher trophic levels, sinking of phytoplankton and faeces may lead to carbon stor-

BGD
doi:10.5194/bg-2015-606

age in sediments, and viral lysis is a major driver of carbon release to dissolved and detrital organic matter (DOM; Wilhelm and Suttle, 1999; Brussaard et al., 2005; Lønborg et al., 2013). Through viral lysis the cell content of the host is released into the surrounding water and utilized by heterotrophic bacteria, thereby stimulating the microbial loop (Brussaard et al., 2008; Sheik et al., 2014). Viral lysis has been found to be at least as important a loss factor as microzooplankton grazing for natural phytoplankton (Baudoux et al., 2006; Mojica et al., 2015a). Any potential changes in the share of grazing and viral lysis will affect the structure and function of the ecosystem. The effect of ocean acidification on these key loss processes is understudied (Rose et al., 2009; Suffrian et al., 2008), to our knowledge no viral lysis rates have been reported. Bacteria may also be affected either directly by OA, or indirectly via changes in the quality or quantity of DOM (Weinbauer et al., 2011). The DOM pool will be affected by any changes in viral lysis rates of phytoplankton or in algal exudation which may increase under low nutrient, high CO_2 conditions (Engel, 2002; Engel et al., 2004). Bacteria are a main food source for microzooplankton (Kuosa and Kivi, 1989) and are also readily infected by viruses, their lysis contributing to the DOM pool (Middelboe and Lyck, 2002).

Overall, community composition and the balance of growth and losses will determine the flow of carbon through the food web and the fate of organic matter with consequences for biogeochemical cycling. This key knowledge is still lacking for most ecosystems, particularly for coastal brackish phytoplankton communities. Here we report on the temporal dynamics of microbes (phytoplankton, heterotrophic prokaryotes and viruses) under the influence of enhanced CO_2 and in relation to viral lysis and grazing top-down control. Using large mesocosms at in situ light and temperature, the Baltic Sea pelagic microbial community was exposed to a range of increasing CO_2 from ambient to future and far-future concentrations. No nutrients were added in order to resemble the natural bottom-up environmental conditions. During the 43 day long experiment the phytoplankton community showed distinct responses to the treatment conditions.

BGD
doi:10.5194/bg-2015-606

2 Materials and Methods

2.1 Study site and experimental set-up

The study was conducted in the Tvärminne Storfjärden (59°51.5′ N, 23°15.5′ E) between 14 June and 7 August 2012. Nine mesocosms each enclosing ~ 55 m^3 of water with a depth of 17 m were moored in a square arrangement within the archipelago. The experimental set-up, carbonate chemistry dynamics and nutrient concentrations throughout the experiment are described in detail by Paul et al. (2015 this issue). After deployment the mesocosms were kept open for 5 days with 3 mm mesh screening over the top and bottom openings before being closed at the bottom and pulled above the sea surface at the top. PAR transparent plastic hoods (open on the side) prevented rain and bird droppings from entering the mesocosms. Six mesocosms were sampled for the current study, unfortunately three were lost due to leakage. Initial fugacity of CO_2 (fCO_2) was 240 µatm and raised to 293 (mesocosm M1), 294 (M5), 488 (M7), 1011 (M6) and 1322 µatm (M3) at day 4. Throughout this study we refer to fCO_2 which takes into account the non-ideal behavior of CO_2 gas and is the standard measurement required for gas exchange calculations (Pfeil et al., 2013). fCO_2 was 0–0.7 % lower than the partial pressure of CO_2 (pCO_2).

For CO_2 manipulations, natural seawater was saturated with CO_2 and then injected evenly throughout the whole depth of the mesocosms in four steps between days 0 to 3 until target fCO_2 was reached. On day 15 a further CO_2 addition was made to the top 7 m of mesocosms, 3, 6 and 8 to replace CO_2 lost due to outgassing. The remaining mesocosms received similar treatment without CO_2. Initial nutrient concentrations, i.e. dissolved inorganic nitrate, phosphate, silicate and ammonium, were 0.05, 0.15, 6.2 and 0.2 (µmol L^{-1}), respectively, and stayed low during the duration of the experiment (Paul et al., 2015 this issue). Salinity was around 5.7, temperature was initially ≈ 8 °C and rose to ≈ 15 °C on day 15 before falling to ≈ 8 °C again.

Collective sampling was performed daily in the morning, using an integrated water sampler, from the top (0–10 m) and from the whole water column (0–17 m) of all

BGD
doi:10.5194/bg-2015-606

mesocosms and the surrounding water. Subsamples were obtained for enumeration of phytoplankton, heterotrophic prokaryotes and viruses. Samples for viral lysis and grazing were taken from 5 m depth using a gentle vacuum-driven pump system. Samples were protected against daylight and warming by thick black plastic bags containing wet ice. In the laboratory the samples were processed at in situ temperature and dimmed light. As viral lysis and grazing rates were determined from samples taken from 5 m depth, samples for microbial abundances reported were taken from the top 10 m integrated samples. For abundances from 0–17 m and the surrounding water see Table S1 and Fig. S1 in the Supplement.

The experiment has been divided into 4 phases based on major physical and biological changes occurring (Paul et al., 2015). Phase 0 before CO_2 addition (days −5 to 0), phase I (days 1–16), phase II (days 17–22) and phase III (days 23–43). Throughout this study the data are presented using 3 colors (blue, grey and red), representing low (mesocosms M1 and M5) intermediate (M6 and M7) and high (M3 and M8) fCO_2 additions.

2.2 Microbial abundances

Microbes were enumerated using a Becton Dickinson FACSCalibur flow cytometer (FCM) equipped with a 488 nm argon laser. The photoautotrophic cells (< 20 µm) were counted directly fresh and were discriminated by their autofluorescent pigments (Marie et al., 1999). The samples were held on wet ice in the dark until counting. Based on their chlorophyll red autofluorescence and the presence of phycoerythrin orange autofluorescence in combination with side scatter signal, the phytoplankton community could be divided into 6 clusters. Phytoplankton cell size of the different phytoplankton clusters was determined by gentle filtration through 25 mm diameter polycarbonate filters (Whatman) with a range of pore sizes (12, 10, 8, 5, 3, 2, 1, and 0.8 µm) according to Veldhuis and Kraay (2004). Average cell sizes of the different phytoplankton groups were 1, 1, 3, 2.9, 5.2, and 8.8 µm diameter for the prokaryotic cyanobacteria *Synechococcus* spp. (SYN), picoeukaryotic phytoplankton I, II and III (Pico I–III), and na-

BGD
doi:10.5194/bg-2015-606

noeukaryotic phytoplankton I, and II (Nano I, II), respectively. Pico III was discriminated from Pico I (comparable average cell size) by the higher orange autofluorescence. Algal particulate organic carbon (POC) was calculated from cell diameters and abundances assuming the cells to be spherical and to contain 0.2 pg C μm^{-3} (Waterbury et al., 1986). Net growth and loss rates of phytoplankton and heterotrophic prokaryotes were derived from exponential regression analysis of the cell abundances.

Abundances of prokaryotes and viruses were determined from 0.5 % glutaraldehyde fixed, flash frozen (−80 °C) samples according to Marie et al. (1999) and (Brussaard (2004), respectively. The prokaryotes include bacteria, archaea and unicellular cyanobacteria, the latter accounting for maximal 10 % of the total abundance, therefore we use the term heterotrophic prokaryotes (HP) in this report.

Briefly, thawed samples were diluted with sterile autoclaved Tris-EDTA buffer (10 mM Tris-HCl and 1 mM EDTA, pH 8.2) and stained with the green fluorescent nucleic acid-specific dye SYBR-Green I (Molecular Probes, Invitrogen Inc.) to a final concentration of 1×10^{-4} (HP) or 0.5×10^{-4} (viruses) of the commercial stock. Virus samples were stained at 80 °C for 10 min and then allowed to cool for 5 min at room temperature in the dark, HP were stained for 15 min at room temperature in the dark (Brussaard, 2004 with adaptation according to Mojica et al., 2014). HP and viruses were discriminated in bivariate scatter plots of green fluorescence vs. side scatter. Final counts were corrected for blanks prepared and analysed like the samples. Two groups of HP were identified as low (LDNA) and high DNA (HDNA) fluorescence HP by their stained nucleic acid fluorescence. Four viral groups (V1–4) were distinguished, whereby V1–V3 showed increasing green nucleic acid fluorescence (with similar side scatter signatures) and cluster V4 had similar green fluorescence to V3 but had higher side scatter similar to a virus infecting nano-eukaryotic algae (Baudoux and Brussaard, 2005).

2.3 Viral lysis and grazing

Microzooplankton grazing and viral lysis of phytoplankton was determined using the dilution method of Landry and Hassett (1982). All seawater handling was performed

BGD
doi:10.5194/bg-2015-606

at in situ temperature under dim light conditions using nitrile gloves. Briefly, one of two series of dilutions of 20, 40, 70 and 100 % whole seawater (200 µm mesh sieved), was gently mixed with 0.45 µm filtered seawater (i.e. microzooplankton grazers removed) and the second series with 30 kDa filtered seawater (i.e. grazers and viruses removed). The dilution reduced the grazing and lysis pressure in a serial manner and regression analysis allowed loss rates (slope) and gross phytoplankton growth rates, in the absence of grazing and lysis (intercept y axis 30 kDa series), to be determined. The 0.45 µm filtrate was produced by gravity filtration of 200 µm mesh sieved seawater through a 0.45 µm Sartopore capsule filter. The 30 kDa ultrafiltrate was produced by tangential flow filtration of 200 µm pre-sieved seawater using a 30 kDa Vivaflow 200 PES membrane tangential flow cartridge (Vivascience). Incubations were set up in triplicate in clear 1.2 L polycarbonate bottles. They were suspended close to the mesocosms in small cages at 5 m depth for 24 h. Subsamples were taken at 0 and 24 h, and phytoplankton abundances of the grazing series (0.45 µm diluent) was enumerated fresh by FCM. Due to time constraint, samples from the 30 kDa series were fixed to a 1 % final concentration with formaldehyde : hexamine solution (18 % v/v : 10 % w/v), stored for 30 min at 4 °C, flash frozen in liquid nitrogen and stored at −80 °C until flow cytometry analysis. The effects of fixation were tested periodically by running duplicate series fresh and frozen. Incubation experiments were run with samples from mesocosm 1 (control) and 3 (high fCO_2); due to the logistics of handling times it was not possible to do more. Experiments were performed until day 31.

Viral lysis of HP was determined by the method of Winget et al. (2005) adapted from the original method by Wilhelm et al. (2002). Here free viruses are removed from a sample of HP, samples are then taken every 3 h for 24 h for virus enumeration. Any viruses in the samples must come from lysing bacteria and thus the rate of bacterial lysis can be estimated using an appropriate burst size. Briefly, free viruses were removed from a 300 mL sample of whole water by re-circulation over a 0.2 µm pore size polyether sulfone membrane (PES) tangential flow filter (Vivaflow 50, Vivascience) at a filtrate expulsion rate of 40 mL min^{-1}. A total of 900 mL of virus-free seawater, freshly pro-

BGD
doi:10.5194/bg-2015-606

duced by 30 kDa ultrafiltration using a PES membrane (Vivaflow 200, Vivascience) was added in three steps to wash away free viruses. Finally the sample was diluted back to the original 300 mL volume with virus-free seawater. The samples were aliquoted into six 50 mL polycarbonate tubes. Mytomycin C (Sigma-Aldrich) (final concentration, 1 µg mL^{-1}, maintained at 4 °C), which induces lysogenic bacteria (Weinbauer and Suttle, 1996) was added to three of the six tubes for each mesocosm studied. A third series of incubations with 0.2 µm filtered samples, the filtrate from the previous step, and thus only free viruses present, was used as a control for viruses adhering to the tube walls. Viruses were found not to be lost from the 0.2 µm controls. At the start of the experiment, 1 mL subsamples were immediately removed from each tube and fixed as previously described for viral and bacterial abundance. The samples were incubated at in situ temperature in the dark and 1 mL subsamples were then taken after 3, 6, 9, 12 and 24 h. Viruses were later enumerated by the method of Brussaard (2004) to determine their rate of production over time. Virus production was determined from linear regression of virus abundance over time (time period used for regression analysis may vary between sampling days, depending on the temporal virus abundance dynamics). Although experiments were performed with mesocosms 1, 2, and 3 as low, mid and high CO_2, mesocosm 2 was lost due to leakage, due to logistical reasons we were only able to perform these assays until day 21.

To determine grazing rates on HP, fluorescently labelled bacteria (FLB) were prepared from cultured *Halomonas halodurans* labelled with 594,6-Dichlorotriazinyl Aminofluorescein (DTAF, 40 µg mL^{-1}) according to Sherr and Sherr (1993). Frozen ampoules containing prey (1 % of total bacteria) were added to triplicate 1 L incubation bottles containing whole water gently passed through 200 µm mesh. Twenty milliliter samples were taken immediately (0 h) and the headspace was removed by gently squeezing the bottle so that no air bubble remained. The samples were fixed with 1 % final concentration 0.2 µm filtered gluteraldehyde (EM-grade, 25 %) and stained with 0.2 µm filtered (Acrodisc® 25 mm Syringe filters, PALL Life Sciences) 4′,6-diamidino-2-phenylindole (DAPI) at a final concentration of 2 µg mL^{-1} (Sherr et al., 1993). Samples

BGD
doi:10.5194/bg-2015-606

were incubated for 30 min at 4 °C and stored in the dark. The 1 L bottles were incubated on a slow turning wheel (1 rpm) at in situ light and temperature conditions for 24 h. 24 h samples were then taken in the same manner as for 0 h. Samples were filtered onto 25 mm, 0.2 µm black polycarbonate filters (GE Healthcare life sciences), mounted on microscopic slides and stored at −20 °C until analysis. FLBs present on a ≈ 0.75 mm^2 area were counted using a Zeiss Axioplan 2 microscope. Grazing (μ) was measured according to

$$N_{T24} = N_{T0} \times e^{-\mu t}$$

Where N_{T24} and N_{T0} are the number of FLBs present at 24 and 0 h, respectively.

2.4 Statistics

Microzooplankton grazing rates were estimated from the regression coefficient of the apparent growth rate vs. fraction of natural seawater for the 0.45-µm series, with the combined rate of viral-induced lysis and microzooplankton grazing being estimated from a similar regression for the 30 kDa series (Baudoux et al., 2006; Kimmance and Brussaard, 2010). A significant difference between the two regression coefficients (as tested by analysis of covariance) indicated a significant viral lysis rate. Phytoplankton gross growth rate, in the absence of grazing and viral lysis, was derived from the y intercept of the 30 kDa series regression. Similarly significant differences between mesocosms M1 and M3 were determined by analysis of covariance of regression lines of the dilution series for the two mesocosms. Students T tests were used to determine significant differences between mesocosms for other parameters.

BGD
doi:10.5194/bg-2015-606

3 Results

3.1 Phytoplankton population dynamics

Phytoplankton showed two main peaks in abundance, at the start of the experiment (day 4 phase I) and day 24 (phase II; Fig. 1a). At the end of phase I the high fCO_2 mesocosms displayed higher phytoplankton abundance than the present day (low) CO_2, whereas the opposite was found for days 17–22. These trends were largely due to the prokaryotic cyanobacteria *Synechococcus* spp., making up on average 74 % of total abundance. In contrast, the total eukaryotic phytoplankton showed a strong positive effect of CO_2 (Fig. 1b), due to the responses of Pico I and II. For all groups, except *Synechococcus* and Pico III, we found that the algal abundances in the surrounding water (Table S1) were more similar to the low fCO_2 than the high fCO_2 mesocosms, demonstrating that the differences between the low and high fCO_2 mesocosms are the effect of the elevated CO_2. Phytoplankton, HP and viral abundances in the 0–17 m samples were generally lower but showed similar dynamics (Figs. S1 and S2 in the Supplement).

3.1.1 *Synechococcus*

SYN showed an initial peak in abundance on day 4 (Fig. 2a), then abundances declined, most so for the low fCO_2 mesocosms, the net growth rate being highly negatively correlated with fCO_2 (R^2 = 0.98, Fig. 2c). The loss measurements (only grazing, no viral lysis detected) confirmed that the total loss rate for the low fCO_2 mesocosm M1 was significantly higher than for the high fCO_2 mesocosm M3 on day 10 (0.56 vs. 0.27 d^{-1}), whilst the gross growth rate did not differ significantly (Fig. 2b). Net increase in cell abundance regained at day 12, for the low CO_2 mesocosms this continued until the bloom at day 24, whilst the high CO_2 mesocosms peaked at day 15 and then dropped again before increasing from day 19–24. Despite the deviation in temporal dynamics between the treatments, SYN abundance peaked at day 24 in all mesocosms

BGD
doi:10.5194/bg-2015-606

with around 4.5×10^5 cells mL^{-1} (Fig. 2a) and were negatively correlated with fCO_2 ($R^2 = 0.77$). For the low fCO_2 mesocosms total net production was higher than for the higher fCO_2 mesocosms as they started lower (day 13) and ended higher (day 24; Fig. 2a). This could be explained by a higher total loss rate for M3 than M1 on day 17 (0.33 vs. 0.17). The decline following (days 24–28) seemed largely due to reduced gross growth rates (Fig. 2b). Thereafter the trend was not so clear until end of experiment.

3.1.2 Picoeukaryotes I

Pico I was numerically the second most dominant group of phytoplankton, 26 % of total phytoplankton abundances on average in the high CO_2 mesocosms and 21 % in the low CO_2 mesocosms. This amounts to 15 % of total POC at high CO_2, 10 % at low CO_2 (mean of total POC). The initial increase (peak in abundance at day 5, Fig. 3a) of these small-sized (mean cell diameter ≈ 1 µm, comparable to SYN) phytoplankton already showed a slight positive trend and strong correlation with fCO_2 for the net growth rate (Fig. 3c, $R^2 = 0.95$) and abundance (Fig. 3f, $R^2 = 0.8$). The higher total net loss rates (days 5 to 9; Fig. 3d) induced a decrease in abundance, which was stronger for the low fCO_2 mesocosms (as illustrated by M1) due to the significantly higher gross growth rates for the high fCO_2 mesocosm (represented by M3; Fig. 3b). The positive correlation of Pico I peak abundance with fCO_2 on day 13 (Fig. 3g, $R^2 = 0.94$) was lost upon another decline in net abundance. Significantly higher losses at high CO_2, a combination of grazing and lysis, resulted in a more dramatic crash at high CO_2 and abundances becoming similar again around day 17 (Fig. 3a). Viral lysis was a significant loss factor compared to grazing, i.e. overall on average 45 and 70 % of total losses in M1 and M3, respectively (Table S2 in the Supplement). An extra addition of CO_2 was given to M3, M6 and M8 because their CO_2 concentration had approached that of the remaining mesocosms. This may have stimulated the gross growth in M3 as compared to M1 (day 19; Fig. 3b) for a longer period in the high

BGD
doi:10.5194/bg-2015-606

fCO_2 mesocosms, this accompanied by higher losses at low CO_2 resulted in a positive correlation of net growth rates with fCO_2 (Fig. 3e, $R^2 = 0.71$) and almost 2 fold higher net abundances at day 21 (Fig. 3a) correlating with fCO_2 (Fig. 3h, $R^2 = 0.84$). Pico I was thus greatly stimulated by increased CO_2, from day 3 throughout the experiment. Standing stock of Pico I remained higher at high CO_2 for the further duration of the experiment (Fig. 3a), with gross growth matched by total losses (Fig. 3b). Surprisingly the higher abundances did not stimulate higher losses during this period, grazing rates were very low in both M1 and M3 and viral lysis was totally responsible for losses on day 31 in both mesocosms (Table S2).

3.1.3 Picoeukaryotes II

A group of larger picoeukaryotes, Pico II (mean diameter of 3 µm) bloomed exactly during the period Pico I was low in standing stock (days 13–21, Fig. 4a) and the peak abundance (day 17) correlated positively with fCO_2 (Fig. 4d). High total losses (0.46 and 0.58 d^{-1} on average days 6–13, in the low and high CO_2 mesocosms respectively) accompanied the high gross growth rates (0.69 and 0.72 d^{-1}) for the same period (Fig. 4b), are indicative of high turnover and explain the slow increase in cell abundance until day 13 (Fig. 4a). During the bloom period of Pico II, losses were smaller than the gross growth rate, more so it seems for M3 than M1 (Fig. 4b). Resultant net growth rates correlated with fCO_2 (Fig. 4c, $R^2 = 0.82$) with peak abundances 1.4 fold higher at high CO_2 (Fig. 4a). Higher losses at high CO_2 then contributed to the faster decline in abundances at high CO_2. Phase III was a period of low turnover for Pico II with low gross growth and loss rates resulting in quite stable cell abundances, still higher at high CO_2, until day 29 after which they declined in all mesocosms (Fig. 4a).

3.1.4 Picoeukaryotes III

Another group with around 2.9 µm cell diameter could be discriminated from Pico II by its higher orange autofluorescence mainly, and as such may represent small-sized

BGD
doi:10.5194/bg-2015-606

cryptophytes. This is just at the lower size range of small cryptophyte (Klaveness, 1989). This group (Pico III) had its highest abundances during phases II and III (days 17–43, Fig. 5a), with a distinct negative correlation to fCO_2 (Fig. 5d, $R^2 = 0.91$). Already directly upon the first CO_2 addition (days 0–4) the abundances declined for the high fCO_2 mesocosms (Fig. 5a) with net growth rates negatively correlated to CO_2 (Fig. 5c, $R^2 = 0.94$). Gross growth rates were indeed significantly higher for M1 than M3 at days 1, 4, and 10 (Fig. 5b). Abundances of the Pico III group in the ambient Fjord water followed the low fCO_2 mesocosms perfectly during this first period, indicating that the crash in the high fCO_2 mesocosms was indeed a direct (negative) effect of CO_2 (Table S1). A similar response of Pico III abundance halting in the high fCO_2 mesocosms and strongly increasing in the low fCO_2 mesocosms occurred directly after the additional CO_2 purge (day 15). Losses were largely due to microzooplankton grazing. Unfortunately about half of the loss assays in the second half of the experiment failed (for unknown reasons), yet the successful assays suggest that losses were minor (Fig. 5b). There may also be larger cryptophytes present in the community, not counted by the flow cytometer because our data show Pico III most dominant in phase III whilst the specific pigment data shows a decline in cryptophytes from phase 0–III (Paul et al., 2015).

3.1.5 Nanoeukaryotes I

The nanoeukaryotes group Nano I consisted of cells with a mean diameter of 5.2 µm and were found with maximum abundances of $5.5 \times 10^2\,mL^{-1}$ (Fig. 6a). After an initial peak at day 6, the lower fCO_2 mesocosms showed the highest numbers at day 17 (Fig. 6a). This seems initiated by 2.3-fold increased total loss rates for M3 than M1 on days 6 and 10 (Fig. 6b) in combination with 2-fold lower gross growth rates on day 10 (Fig. 6b) leading to net growth correlating negatively with CO_2 days 10–12 (Fig. 6c, $R^2 = 0.83$). Viral lysis occurred largely in the high CO_2 mesocosm throughout the experiment with rates ranging from 0.13 to $0.7\,d^{-1}$ (making up 16 to 98 % of total

BGD
doi:10.5194/bg-2015-606

losses Table S2). Lower total loss rates at days 13 and 17 in both mesocosms allowed a small increase in abundance, peaking on day 17 and negatively correlated to fCO_2 (Fig. 6d, $R^2 = 0.67$).

3.1.6 Nanoeukaryotes II

The temporal dynamics of Nano II were rather erratic (Fig. 7a). Nano II were the largest in size and may have been made up by different phytoplankton species, however due to their low numbers we were unable to discriminate separate groups. The peak in abundance at day 16 showed a negative correlation to fCO_2 (Fig. 7d, $R^2 = 0.61$), and was the result of an overall reduced net growth rate with fCO_2 (Fig. 7c, $R^2 = 0.56$). The subsequent decline seems the result of reduced gross growth rate (to even zero) and increased loss rate (day 20; Fig. 7b).

3.1.7 Algal POC

The calculated mean algal POC shows that CO_2 had a clear positive effect on the biomass of Pico I and II (Fig. 8a; $p < 0.0001$). The effect became noticeable already after a few days into the experiment and the mean Pico I and II POC concentration in the high fCO_2 mesocosms stayed high during the entire duration of the experiment. At the same time the remaining algal groups showed reduced POC at enhanced CO_2 (the sum of Pico III, and Nano I and II and *Synechococcus*; Fig. 8b, $p < 0.01$). Particularly Pico III showed a nearly instant and markedly negative response to increased CO_2 concentration (Fig. S3a in the Supplement). This was a lasting effect as the strongest difference was found in the second half of the experiment. For Nano I and II the higher algal POC concentrations became only more apparent at the end of phase I (days 10–16; Fig. S3b). Due to its small cell size, the numerically dominant SYN accounted on average for 40 % of total POC. We are aware that due to the exclusion of 3 mesocosms (see Sect. 2), the number of fCO_2 treatments is reduced to 6, which limits the

BGD
doi:10.5194/bg-2015-606

statistical power of the results. Still, our data show that the responses of the different phytoplankton groups to ocean acidification were evident and consistent.

3.2 HP population dynamics

In general HP abundance followed the total algal biomass, with an initial increase during the first days following the closure of the mesocosms (Fig. 9a). The increase was mainly due to the HDNA-HP (Fig. 9b). There was no significant difference in HP abundance between the treatments at the first peak, however, grazing was significantly higher and at the same time viral lysis was slightly lower in the low (M1) as compared to the high CO_2 mesocosm (M3) (Figs. 10a and b). The decline in HP abundance from days 5 to 9 seemed due to declining phytoplankton biomass (Fig. 1a) and increasing viral lysis rates (12–16 % d^{-1} representing 39 % of total losses in M1 and 37 % in M3 on day 11, Fig. 10b).

From days 10–15 HP dynamics became clearly affected by fCO_2 with significantly higher abundances and net growth rates at higher CO_2 (Fig. 9a) although we cannot exclude an indirect response due to altered algal dynamics in response to higher fCO_2. Both the HDNA and the LDNA-HP (peak abundance on day 13, Fig. 9b and c) showed significant correlation with fCO_2 (R^2 = 0.92 and 0.79 respectively, total HP R^2 = 0.88, Fig. 10c). In the higher fCO_2 mesocosms the decline in HP abundance following the peak at day 13 was largely the result of decreasing HDNA-HP numbers (Fig. 9b). Grazing was indeed significantly higher in the high CO_2 mesocosm M3 but the data for viral lysis were inconclusive due to a failed assay for M1 at day 14 (Fig. 10a and b). The significantly ($p < 0.01$) higher viral abundances, particularly due to the V3 group, with highest green fluorescence, for the high CO_2 mesocosms (Fig. 11a and b) around that time do seem to indicate that viral lysis in the high CO_2 mesocosms was higher.

During phase II HP abundances increased steadily until day 24 (for both HDNA and LDNA), corresponding to increased algal biomass (Fig. 1) and low grazing rates (0.1–0.2 d^{-1}; Fig. 10a). Although the overall higher HP standing stock in the low CO_2 mesocosms was due to enhanced growth around day 16 (Fig. 9a) the net growth rates were

BGD
doi:10.5194/bg-2015-606

comparable after day 17. Moreover, the higher abundances were only found for the HDNA-HP (Fig. 9b and c). Viral lysis rates seem higher for the low CO_2 mesocosms (Fig. 10b). The higher HP abundances in the low fCO_2 mesocosms seem thus merely due to the lower grazing prior to the increase, i.e. at the end of phase I (day 14).

HP abundance ultimately declined again (from days 28–35), but in M1 less than in the other mesocosms (Fig. 9a). We unfortunately have no data of the HP loss rates after day 25, however viral abundances increased at a steady rate of 2.2×10^6 d^{-1} (to a maximum of 0.9^8 mL^{-1} by day 39; Fig. 11a), implying that viral lysis was at least partly responsible for the decline in HP abundance. There was no significant difference in viral abundances between the treatments during this period. Estimating the viral burst size from the increase in viral abundance and concomitant decline in bacterial abundance gives on average 30 viruses per lysed bacterial cell.

4 Discussion

The summer phytoplankton community was dominated by small-sized phytoplankton of which picoeukaryotic photoautotrophs Pico I and II showed a very strong fertilization effect with enhanced fCO_2 directly following the initial CO_2 additions until the end of the experiment. At the same time, the rest of the phytoplankton (Pico III, Nano I and II, and the prokaryote *Synechococcus* spp.) showed reduced abundances at higher fCO_2. These shifts in community structure could be explained by examining the gross growth rates in combination with the losses of the individual groups. HP abundances followed in general algal biomass dynamics and at times were related to viral lysis of phytoplankton groups. Viruses overall followed HP population dynamics.

4.1 Phase 0 (days −5 to 0), before CO_2 addition

At the start of the experiment the trophic conditions were typical for the Baltic Sea in summer, low in nitrate but with phosphate and silicate non-limiting (Paul et al., 2015). In

BGD
doi:10.5194/bg-2015-606

most experimental work nutrients have been added to stimulate phytoplankton growth, therefore little data exists for oligotrophic phytoplankton communities (Brussaard et al., 2013), in which smaller sized algae, which are better competitors for nutrients tend to dominate (Raven, 1998; Veldhuis et al., 2005). From the start of the experiment the flow cytometric phytoplankton community (< 20 µm cell diameter) was dominated by *Synechococcus* spp. (SYN) and the smallest picoeukaryotes, (Pico I; both around 1 µm). Picoeukaryotes are found in high numbers at this site throughout the year and *Synechococcus* only in summer (Kuosa, 1991). Microscopic identification of picoeukaryotes is extremely difficult and no species have been described for the region (Kuosa, 1991), however, pigment analyses suggest that Pico I and II are likely to be prasinophytes or other chlorophytes (Paul et al., 2015). Biomass of *Synechococcus* and Pico I increased steadily upon closure of the mesocosms due to high gross growth rates whilst the other groups dropped slightly in abundance. Our grazing rates of *Synechococcus* compare well to the average reported estimate of grazing on cyanobacteria in July in this region of 0.3 d^{-1} (range 0.18–0.53 d^{-1}, Kuosa, 1991). HP also increased, at rates of 0.22 d^{-1} and 0.14 d^{-1} for the high and low DNA (HDNAHP and LDNAHP), respectively, similar to rates reported for this region (Kuosa, 1991). Grazing rates were around 0.3–0.5 d^{-1} with viral lysis rates of < 2 % d^{-1}, indicating that bacterial production rates must have been around 0.6 d^{-1}.

4.2 Phase I (days 1–16)

According to Paul et al. (2015) this phase was characterised by high productivity and high organic matter turnover. Indeed we saw all phytoplankton groups bloom and we measured relatively high losses by grazing and viral lysis for all groups during phase I, responsible for the referred high turnover of organic matter. Certainly HP responded positively to the increased algal productivity and viral lysis. More specifically, during phase I Pico I benefitted directly and most from enhanced CO_2 as demonstrated by their significantly ($p < 0.05$) higher gross growth rates. Also Pico II showed positively

BGD
doi:10.5194/bg-2015-606

correlated net growth rates with CO_2 enrichment, but somewhat later into phase I (days 12–17) due to reduced losses.

The stimulation of Pico I by elevated CO_2 may be due to a stronger reliance on diffusive CO_2 entry compared to larger cells. Model simulations reveal that whilst near-cell CO_2/pH conditions are close to those of the bulk water for cells < 5 µm in diameter, they diverge as cell diameters increase (Wolf-Gladrow and Riebesell, 1997; Flynn et al., 2012). This is due to the size-dependent thickness of the diffusive boundary layer, which determines the diffusional transport across the boundary layer and to the cell surface (Wolf-Gladrow and Riebesell, 1997; Flynn et al., 2012). It is suggested that larger cells may be more able to cope with pCO_2 variability as their carbon acquisition is more geared towards dealing with low CO_2 concentrations in their diffusive boundary, e.g. by means of active carbon acquisition and bicarbonate utilization (Wolf-Gladrow and Riebesell, 1997; Flynn et al., 2012). However, as the Baltic Sea experiences particularly large seasonal fluctuations in pH and pCO_2 (Jansson et al., 2013) due to the low buffering capacity of the waters, phytoplankton here may be expected to have a high degree of physiological plasticity. Previous mesocosm studies have reported enhanced abundances of the picoeukaryotic photoautotroph *Micromonas pusilla* at higher CO_2 (Engel et al., 2007; Meakin and Wyman, 2011; Maat et al., 2014). Another summer mesocosm study in the Arctic revealed that even smaller picoeukaryotes, similar to Pico I in our study, showed a positive response to enhanced fCO_2 (Brussaard et al., 2013). Furthermore, Schaum et al. (2012) found that 16 ecotypes of *Ostreococcus tauri* (also similar in size to Pico I) increased in growth rate by 1.4–1.7 fold at 1000 µatm pCO_2. All ecotypes increased their photosynthetic rates and those with most plasticity, most able to vary their photosynthetic rate in response to changes in CO_2, were most likely to increase in frequency in the community. It is likely that the picoeukaryotes in our study, which show stimulation by CO_2 are adapted to a highly variable carbonate system regime and are able to increase their photosynthetic rate when additional CO_2 is available.

BGD
doi:10.5194/bg-2015-606

A net loss of 60 % of the mean standing stock of Pico I at low, and 42 % at high CO_2 after day 5 was likely due to grazing, on average 0.26 d^{-1}, and lysis 0.18 d^{-1} (lysis in M3 only). In general, grazing was a substantial loss factor for all phytoplankton groups during this period and additionally Pico I and II, Nano I and II experienced noteworthy viral mediated mortality. The high grazing rates coincided with high abundances of the ciliate *Myrionecta rubra* at the start of the experiment (Lischka et al., 2015). After day 10 abundances of most of the phytoplankton groups increased, corresponding with a decline in abundance of this ciliate (Lischka et al., 2015). Occasionally grazing rates between the high CO_2 (M3) and present-day, low CO_2 (M1) mesocosms differed significantly although no general trend could be observed.

For Nano I and Nano II the gross growth rates seemed to increase at higher fCO_2, but at the same time the losses also increased. However, differences in growth and loss rates were not statistically significant and thus it stays difficult to underpin why these phytoplankton groups peaked to higher abundances at lower CO_2 in phase I. Potentially released competition for nutrients towards the end of phase I (the numerically dominant Pico I and SYN had declined in abundance by then) aided the increase of the nanoeukaryotes.

During Phase I HP increased in net abundance which matched the increase in algal biomass. This increase was initially tempered by grazers, and additionally viral lysis became increasingly important (to 60 % of total losses at the end of phase I). HP were significantly more abundant at high CO_2 during the second half of phase I. This may be due to increased availability of organic carbon at high CO_2 due to higher rates of viral lysis of phytoplankton. We measured higher lysis rates in the high CO_2 mesocosm (M3) than in the control (M1) on day 6 for Pico II and Nano I and on day 10 for Pico I and II, Nano I and II at higher CO_2. Stimulation of HP abundances was seen in a previous mesocosm campaign apparently due to higher availability of TEP and aminopeptidase activity (Endres et al., 2014). Increased TEP production is often associated with low nutrient, high CO_2 conditions (Weinbauer et al., 2011).

BGD
doi:10.5194/bg-2015-606

Mean virus abundances increased at higher CO_2 levels during phase I, which is likely a response to increased phytoplankton and HP biomass. During previous mesocosm studies no direct or indirect effects of CO_2 addition on the abundance of bacteriophages were seen (Paulino et al., 2007; Larsen et al., 2008; Brussaard et al., 2013). Direct effects of higher CO_2 on viruses themselves are not expected as marine virus isolates have been found to be quite stable (both particle and infectivity) over the range of pH obtained in the present study (Mojica and Brussaard, 2014). Besides lytic infection, there is the potential for lysogenic viral life cycle, during which viral DNA is integrated in the host as a prophage (Weinbauer, 2004). We examined whether increased CO_2 concentrations affect the type of viral life cycle but found no evidence lysogeny was affected.

4.3 Phase II (days 17–30)

Phase II displayed a second peak in total phytoplankton abundances related to increased picophytoplankton but reduced nanophytoplankton. Reduced microzooplankton grazing pressure on the picoeukaryotes and *Synechococcus* after day 17, allowed them to increase in net abundance during Phase II. Microzooplankton abundances were reduced as compared to the start of the experiment (approximately an order of magnitude lower) and mesozooplankton increased (Lischka et al., 2015). Thus increased grazing of mesozooplankton on microzooplankton may have resulted in reduced grazing of, and proliferation of, picophytoplankton. Furthermore, higher abundances of the smallest size class of the ciliate *M. rubra* were seen in the higher CO_2 mesocosms (days 19–31, Lischka et al., 2015) which may explain the lower abundances of Pico III due to its ability to "rob" chloroplasts from cryptophytes (Lischka et al., 2015). *M. rubra* abundance decreased from day 3 to day 17, which may be due to the decreased Pico III cryptophyte prey abundances.

Synechococcus bloomed during phase II, with significantly reduced abundances at higher CO_2. So although the Pico I benefitted from CO_2 enrichment, the similar sized *Synechococcus* did not. *Synechococcus* has shown diverse, strain-specific responses

BGD
doi:10.5194/bg-2015-606

to CO_2 enrichment (Fu et al., 2007; Lu et al., 2006; Traving et al., 2014). As a prokaryote, Synechococcus has very different physiology, needing extremely efficient CCMs due to the inefficiency of its Rubisco, which can concentrate CO_2 to up to 1000-fold higher than the external medium (Badger and Andrews, 1982). Thus at current CO_2 concentrations they may attain maximal growth rates (Low-Décarie et al., 2014).

HP abundance increased steadily during Phase II, again matching total phytoplankton dynamics. Following the initially higher HP abundances at higher fCO_2 in Phase I, we found during Phase II (from days 16–25) decreased abundances of HDNA-HP at high CO_2 which fits with the reported reduced bacterial production (Hornick et al., 2015) and respiration measurements (Spilling et al., 2015) in these mesocosms during this time.

4.4 Phase III (days 31–43)

The positive growth response of the picoeukaryotes to earlier CO_2 enrichment was still clearly reflected in Chlorophyll *a* concentration, particulate organic carbon and phosphorus, but also in the dissolved organic carbon (DOC) pools in Phase III (Paul et al., 2015). This increase in DOC at high CO_2 (Paul et al., 2015), may originate from viral lysis of HP and phytoplankton. We measured higher viral lysis rates for SYN, Pico II and Nano I and similar lysis rates but higher standing stock of Pico I at high CO_2 on day 31. Additionally after day 22 total viral abundances increased steadily until the end of the experiment. Alternatively, increased CO_2 coupled with low nutrients can stimulate photosynthetic release of DOC and transparent exopolymer particles (TEP) formation (Engel, 2002; Borchard and Engel, 2012). TEP may promote aggregation and sinking of particulate organic matter (Brussaard et al., 2008; Lønborg et al., 2013) and offset the reduced sedimentation associated with smaller cells. A significant negative correlation was also reported between diatom abundance and CO_2 during phase III (Paul et al., 2015), which is similar to a previous ocean acidification mesocosm experiment (Brussaard et al., 2013). Brussaard et al. (2013) suggested that diatom growth was reduced due to increased uptake of the growth limiting nutrients by the picoeukary-

BGD
doi:10.5194/bg-2015-606

otes at high CO_2 and may result in reduced sedimentation. However, no difference in sedimentation rates was reported between CO_2 treatments for the current study indicating that the change in phytoplankton community composition did not result in altered transport of POC (live or dead) (Paul et al., 2015).

5 Future perspectives

Our study shows that CO_2 enrichment favours the net growth of the very small-sized (1 µm) picoeukaryotic phytoplankton. This positive response with fCO_2 is very specific as neither *Synechococcus* spp. nor of the nanoeukaryotic phytoplankton groups displayed enhanced growth. Increasing CO_2 leads to a number of further global changes, e.g. increasing sea surface temperatures (SST) which in turn increase stratification, reducing nutrient supply in surface waters (Boyd, 2011). Such physiochemical conditions have been reported to favour small cells (Cermeño et al., 2008; Craig et al., 2013; Li et al., 2009; Mojica et al., 2015a, b; Riebesell et al., 2009). Also the activity of HP is expected to be affected by higher SST due to increased enzyme activities, bacterial production, respiration rates, polysaccharide release and TEP formation (Borchard et al., 2011; Engel et al., 2011; Piontek et al., 2009; Wohlers et al., 2009; Wohlers-Zöllner et al., 2011). Enhanced bacterial re-mineralization of nutrients could further increase the autotrophic production by the small-sized phytoplankton (Engel et al., 2013; Riebesell and Tortell, 2011; Riebesell et al., 2009). At the same time, viral lysis and microbial respiration are the main natural sources of atmospheric CO_2 that negatively affect the biological pump (del Giorgio and Duarte, 2002). Overall the evidence suggests that besides CO_2 enrichment favouring small picoeukaryotic phytoplankton, multiple other factors will tend to promote a more regenerative system with potential consequences for ecosystem production and functioning.

BGD
doi:10.5194/bg-2015-606

The Supplement related to this article is available online at doi:10.5194/bgd-13-1-2016-supplement.

Author contributions. Design and overall coordination of research by C. Brussaard. Organization and performance of analyses in the field by K. Crawfurd. Data analysis by K. Crawfurd and C. Brussaard. Coordination of the overall KOSMOS mesocosms project by U. Riebesell. All authors contributed to the writing of the paper.

Acknowledgements. This project was funded through grants to C. Brussaard by the Darwin project, the Netherlands Institute for Sea Research (NIOZ), and the EU project MESOAQUA (grant agreement number 228224). We thank the KOSMOS project organisers and team in particular Andrea Ludwig, the staff of the Tvärminne Zoological Station and the diving team. We give special thanks to Anna Noordeloos, Kirsten Kooiman and Richard Doggen for their technical assistance during this campaign. We also gratefully acknowledge the captain and crew of R/V *ALKOR* for their work transporting, deploying and recovering the mesocosms. The collaborative mesocoms campaign was funded by BMBF projects BIOACID II (FKZ 03F06550) and SOPRAN Phase II (FKZ 03F0611).

References

Badger, M. R., Andrews, T. J., Whitney, S. M., Ludwig, M., Yellowlees, D. C., Leggat, W., and Price, G. D.: The diversity and coevolution of Rubisco, plastids, pyrenoids, and chloroplast-based CO_2-concentrating mechanisms in algae, Can. J. Bot., 76, 1052–1071, 1998.

Barcelos e Ramos, J., Biswas, H., Schulz, K. G., LaRoche, J., and Riebesell, U.: Effect of rising atmospheric carbon dioxide on the marine nitrogen fixer Trichodesmium, Global Biogeochem. Cy., 21, GB2028, doi:10.1029/2006GB002898, 2007.

Baudoux, A. C. and Brussaard, C. P. D.: Characterization of different viruses infecting the marine harmful algal bloom species Phaeocystis globosa, Virology, 341, 80–90, doi:10.1016/j.virol.2005.07.002, 2005.

Baudoux, A. C., Noordeloos, A. A. M., Veldhuis, M. J. W., and Brussaard, C. P. D.: Virally induced mortality of Phaeocystis globosa during two spring blooms in temperate coastal waters, Aquat. Microb. Ecol., 44, 207–217, doi:10.3354/ame044207, 2006.

BGD

doi:10.5194/bg-2015-606

Borchard, C. and Engel, A.: Organic matter exudation by Emiliania huxleyi under simulated future ocean conditions, Biogeosciences, 9, 3405–3423, doi:10.5194/bg-9-3405-2012, 2012.
Borchard, C., Borges, A. V., Händel, N., and Engel, A.: Biogeochemical response of Emiliania huxleyi (PML B92/11) to elevated CO_2 and temperature under phosphorous limitation: a chemostat study, J. Exp. Mar. Bio. Ecol., 410, 61–71, 2011.
Boyd, P. W.: Beyond ocean acidification, Nat. Geosci., 4, 273–274, doi:10.1038/ngeo1150, 2011.
Brussaard, C. P. D.: Optimization of procedures for counting viruses by flow cytometry, Appl. Environ. Microb., 70, 1506–1513, doi:10.1128/AEM.70.3.1506-1513.2004, 2004.
Brussaard, C. P. D., Noordeloos, A. A. M., Sandaa, R. A., Heldal, M., and Bratbak, G.: Discovery of a dsRNA virus infecting the marine photosynthetic protist Micromonas pusilla, Virology, 319, 280–291, doi:10.1016/j.virol.2003.10.033, 2004.
Brussaard, C. P. D., Kuipers, B., and Veldhuis, M. J. W.: A mesocosm study of Phaeocystis globosa population dynamics: I. Regulatory role of viruses in bloom control, Harmful Algae, 4, 859–874, doi:10.1016/j.hal.2004.12.015, 2005.
Brussaard, C. P. D., Wilhelm, S. W., Thingstad, F., Weinbauer, M. G., Bratbak, G., Heldal, M., Kimmance, S. A., Middelboe, M., Nagasaki, K., Paul, J. H., Schroeder, D. C., Suttle, C. A., Vaqué, D., and Wommack, K. E.: Global-scale processes with a nanoscale drive: the role of marine viruses, ISME J., 2, 575–578, doi:10.1038/ismej.2008.31, 2008.
Brussaard, C. P. D., Noordeloos, A. A. M., Witte, H., Collenteur, M. C. J., Schulz, K., Ludwig, A., and Riebesell, U.: Arctic microbial community dynamics influenced by elevated CO_2 levels, Biogeosciences, 10, 719–731, doi:10.5194/bg-10-719-2013, 2013.
Cermeño, P., Dutkiewicz, S., Harris, R. P., Follows, M., Schofield, O., and Falkowski, P. G.: The role of nutricline depth in regulating the ocean carbon cycle., P. Natl. Acad. Sci. USA, 105, 20344–20349, doi:10.1073/pnas.0811302106, 2008.
Craig, S. E., Thomas, H., Jones, C. T., Li, W. K. W., Greenan, B. J. W., Shadwick, E. H., and Burt, W. J.: Temperature and phytoplankton cell size regulate carbon uptake and carbon overconsumption in the ocean, Biogeosciences Discuss., 10, 11255–11282, doi:10.5194/bgd-10-11255-2013, 2013.
Dickinson, G. H., Matoo, O. B., Tourek, R. T., Sokolova, I. M., and Beniash, E.: Environmental salinity modulates the effects of elevated CO_2 levels on juvenile hard-shell clams, Mercenaria mercenaria, J. Exp. Biol., 216(Pt 14), 2607–18, doi:10.1242/jeb.082909, 2013.

BGD
doi:10.5194/bg-2015-606

Endres, S., Galgani, L., Riebesell, U., Schulz, K. G., and Engel, A.: Stimulated bacterial growth under elevated pCO_2: results from an off-shore mesocosm study, PLoS One, 9, e99228, doi:10.1371/journal.pone.0099228, 2014.

Engel, A.: Direct relationship between CO_2 uptake and transparent exopolymer particles production in natural phytoplankton, J. Plankton Res., 24(1), 49–53, doi:10.1093/plankt/24.1.49, 2002.

Engel, A., Delille, B., Jacquet, S., Riebesell, U., Rochelle-Newall, E., Terbrüggen, A., and Zondervan, I.: Transparent exopolymer particles and dissolved organic carbon production by Emiliania huxleyi exposed to different CO_2 concentrations: a mesocosm experiment, Aquat. Microb. Ecol., 34, 93–104, 2004.

Engel, A., Schulz, K. G., Riebesell, U., Bellerby, R., Delille, B., and Schartau, M.: Effects of CO_2 on particle size distribution and phytoplankton abundance during a mesocosm bloom experiment (PeECE II), Biogeosciences, 5, 509–521, doi:10.5194/bg-5-509-2008, 2008.

Engel, A., Händel, N., Wohlers, J., Lunau, M., Grossart, H. P., Sommer, U., and Riebesell, U.: Effects of sea surface warming on the production and composition of dissolved organic matter during phytoplankton blooms: results from a mesocosm study, J. Plankton Res., 33, 357–372, doi:10.1093/plankt/fbq122, 2011.

Engel, A., Borchard, C., Piontek, J., Schulz, K. G., Riebesell, U., and Bellerby, R.: CO_2 increases ^{14}C primary production in an Arctic plankton community, Biogeosciences, 10, 1291–1308, doi:10.5194/bg-10-1291-2013, 2013.

Feng, Y., Leblanc, K., Rose, J. M., Hare, C. E., Zhang, Y., Lee, P. A., Wilhelm, S. W., DiTullio, G. R., Rowe, J. M., Sun, J., Nemcek, N., Gueguen, C., Passow, U., Benner, I., Hutchins, D. A., and Brown, C.: Effects of increased pCO_2 and temperature on the North Atlantic spring bloom, I. The phytoplankton community and biogeochemical response, Mar. Ecol.-Prog. Ser., 388, 13–25, 2009.

Field, C. B., Behrenfeld, M. J., Randerson, J. T., and Falkowski, P.: Primary production of the biosphere: integrating terrestrial and oceanic components, Science, 281, 237–240, doi:10.1126/science.281.5374.237, 1998.

Flynn, K. J., Blackford, J. C., Baird, M. E., Raven, J. A., Clark, D. R., Beardall, J., Brownlee, C., Fabian, H., and Wheeler, G. L.: Letter changes in pH at the exterior surface of plankton with ocean acidification, Nat. Clim. Chang., 2, 510–513, doi:10.1038/nclimate1696, 2012.

Fu, F. X., Warner, M. E., Zhang, Y., Feng, Y., and Hutchins, D. A.: Effects of increased temperature and CO_2 on photosynthesis, growth, and elemental ratios in marine Synechococ-

BGD

doi:10.5194/bg-2015-606

cus and Prochlorococcus (Cyanobacteria), J. Phycol., 43, 485–496, doi:10.1111/j.1529-8817.2007.00355.x, 2007.
Del Giorgio, P. A. and Duarte, C. M.: Respiration in the open ocean, Nature, 420, 379–384, doi:10.1038/nature01165, 2002.
Grob, C., Hartmann, M., Zubkov, M. V., and Scanlan, D. J.: Invariable biomass-specific primary production of taxonomically discrete picoeukaryote groups across the Atlantic Ocean, Environ. Microbiol., 13, 3266–3274, doi:10.1111/j.1462-2920.2011.02586.x, 2011.
Hein, M. and Sand-Jensen, K.: CO_2 increases oceanic primary production, Nature, 388, 526–527, 1997.
Hornick, T., Bach, L. T., Crawfurd, K. J., Spilling, K., Achterberg, E. P., Brussaard, C. P. D., Riebesell, U., and Grossart, H.-P: Effect of ocean acidification on bacterial dynamics during a low productive late summer situation in the Baltic Sea, in preparation, Biogeosciences, 2015.
Hutchins, D. A.: CO_2 control of trichodesmium, Limnol. Oceanogr., 52, 1293–1304, 2007.
IPCC: IPCC Fourth Assessment Report: Climate Change 2007: The Physical Science Basis: Contribution of Working Group I to the Fourth Assessment Report of the Intergovernmental Panel on Climate Change, edited by: Solomon, S., Qin, D., Manning, M., Chen, Z., Marquis, M., Averyt, K. B., Tignor, M., and Miller, H. L., Cambridge University Press, Cambridge University Press, Cambridge, UK and New York, NY, USA., 996 pp., 2007.
Jansson, A., Norkko, J., and Norkko, A.: Effects of reduced pH on Macoma balthica larvae from a system with naturally fluctuating pH-dynamics, PLoS One, 8, e68198, doi:10.1371/journal.pone.0068198, 2013.
Kimmance, S. A. and Brussaard, C. P. D.: Estimation of viral-induced phytoplankton mortality using the modified dilution method, in: Manual of Aquatic Viral Ecology, edited by: Wilhelm, S. W., Weinbauer M. G., and Suttle C. A., Association for the Sciences of Limnology and Oceanography, 65–73, doi:10.4319/mave.2010.978-0-9845591-0-7.65, 2010.
Klaveness, D.: Biology and ecology of the Cryptophyceae: status and challenges, Biol. Ocean., 6, 257–270, 1989.
Kuliński, K. and Pempkowiak, J.: The carbon budget of the Baltic Sea, Biogeosciences Discuss., 8, 4841–4869, doi:10.5194/bgd-8-4841-2011, 2011.
Kuosa, H.: Picoplanktonic algae in the northern Baltic Sea: seasonal dynamics and flagellate grazing, Mar. Ecol.-Prog. Ser., 73(2–3), 269–276, doi:10.3354/meps073269, 1991.

BGD
doi:10.5194/bg-2015-606

Kuosa, H. and Kivi, K.: Bacteria and heterotrophic flagellates in the pelagic carbon cycle in the northern Baltic Sea, Mar. Ecol.-Prog. Ser., 53(1975), 93–100, doi:10.3354/meps053093, 1989.

Landry, M. R. and Hassett, R. P.: Estimating the grazing impact of marine micro-zooplankton, Mar. Biol., 67, 283–288, doi:10.1007/BF00397668, 1982.

Larsen, J. B., Larsen, A., Thyrhaug, R., Bratbak, G., and Sandaa, R.-A.: Response of marine viral populations to a nutrient induced phytoplankton bloom at different pCO_2 levels, Biogeosciences, 5, 523–533, doi:10.5194/bg-5-523-2008, 2008.

Leonardos, N. and Geider, R. J.: Elevated atmospheric carbon dioxide increases organic carbon fixation by Emiliania huxleyi (Haptophyta), under nutrient-limited high-light conditions, J. Phycol., 41, 1196–1203, doi:10.1111/j.1529-8817.2005.00152.x, 2005.

Li, W. K. W., McLaughlin, F. A., Lovejoy, C., and Carmack, E. C.: Smallest algae thrive as the Arctic Ocean freshens, Science, 326, 539 pp., doi:10.1126/science.1179798, 2009.

Lischka, S., Bach, L. T., Schulz, K. G., and Riebesell, U.: Micro- and mesozooplankton community response to increasing levels of fCO_2 in the Baltic Sea: insights from a large-scale mesocosm experiment, Biogeosciences Discuss., 12, 20025–20070, doi:10.5194/bgd-12-20025-2015, 2015.

Lønborg, C., Middelboe, M., and Brussaard, C. P. D.: Viral lysis of Micromonas pusilla: impacts on dissolved organic matter production and composition, Biogeochemistry, 116, 231–240, doi:10.1007/s10533-013-9853-1, 2013.

Low-Décarie, E., Fussmann, G. F., and Bell, G.: Aquatic primary production in a high-CO_2 world, Trends Ecol. Evol., 29, 223–232, doi:10.1016/j.tree.2014.02.006, 2014.

Lu, Z., Jiao, N., and Zhang, H.: Physiological changes in marine picocyanobacterial Synechococcus strains exposed to elevated CO_2 partial pressure, Mar. Biol. Res., 2, 424–430, doi:10.1080/17451000601055419, 2006.

Maat, D. S., Crawfurd, K. J., Timmermans, K. R., and Brussaard, C. P. D.: Elevated CO_2 and phosphate limitation favor micromonas pusilla through stimulated growth and reduced viral impact, Appl. Environ. Microb., 80, 3119–3127, 2014.

Marie, D., Brussaard, C. P. D., Thyrhaug, R., Bratbak, G., and Vaulot, D.: Enumeration of marine viruses in culture and natural samples by flow cytometry, Appl. Environ. Microb., 65, 45–52, 1999.

Meakin, N. G. and Wyman, M.: Rapid shifts in picoeukaryote community structure in response to ocean acidification, ISME J., 5, 1397–1405, 2011.

BGD

doi:10.5194/bg-2015-606

Merkouriadi, I. and Leppäranta, M.: Long-term analysis of hydrography and sea-ice data in Tvärminne, Gulf of Finland, Baltic Sea, Clim. Change, 124, 849–859, doi:10.1007/s10584-014-1130-3, 2014.

Meyer, J. and Riebesell, U.: Reviews and Syntheses: Responses of coccolithophores to ocean acidification: a meta-analysis, Biogeosciences, 12, 1671–1682, doi:10.5194/bg-12-1671-2015, 2015.

Middelboe, M. and Lyck, P. G.: Regeneration of dissolved organic matter by viral lysis in marine microbial communities, Aquat. Microb. Ecol., 27, 187–194, doi:10.3354/ame027187, 2002.

Mojica, K. D. A. and Brussaard, C. P. D.: Factors affecting virus dynamics and microbial host–virus interactions in marine environments, FEMS Microbiol. Ecol., 89, 495–515, doi:10.1111/1574-6941.12343, 2014.

Mojica, K. D. A., Evans, C., and Brussaard, C. P. D.: Flow cytometric enumeration of marine viral populations at low abundances, Aquat. Microb. Ecol., 71, 203–209, doi:10.3354/ame01672, 2014.

Mojica, K. D. A., Huisman, J., Wilhelm, S. W., and Brussaard, C. P. D.: Latitudinal variation in virus-induced mortality of phytoplankton across the North Atlantic Ocean, ISME J, doi:10.1038/ismej.2015.130, 2015a.

Mojica, K. D. A., van de Poll, W. H., Kehoe, M., Huisman, J., Timmermans, K. R., Buma, A. G. J., van der Woerd, H. J., Hahn-Woernle, L., Dijkstra, H. A., and Brussaard, C. P. D.: Phytoplankton community structure in relation to vertical stratification along a north–south gradient in the Northeast Atlantic Ocean, Limnol. Oceanogr., 60, 1498–1521, doi:10.1002/lno.10113, 2015b.

Paul, A. J., Bach, L. T., Schulz, K.-G., Boxhammer, T., Czerny, J., Achterberg, E. P., Hellemann, D., Trense, Y., Nausch, M., Sswat, M., and Riebesell, U.: Effect of elevated CO_2 on organic matter pools and fluxes in a summer Baltic Sea plankton community, Biogeosciences, 12, 6181–6203, doi:10.5194/bg-12-6181-2015, 2015.

Paulino, A. I., Egge, J. K., and Larsen, A.: Effects of increased atmospheric CO_2 on small and intermediate sized osmotrophs during a nutrient induced phytoplankton bloom, Biogeosciences Discuss., 4, 4173–4195, doi:10.5194/bgd-4-4173-2007, 2007.

Pfeil, B., Olsen, A., Bakker, D. C. E., Hankin, S., Koyuk, H., Kozyr, A., Malczyk, J., Manke, A., Metzl, N., Sabine, C. L., Akl, J., Alin, S. R., Bates, N., Bellerby, R. G. J., Borges, A., Boutin, J., Brown, P. J., Cai, W.-J., Chavez, F. P., Chen, A., Cosca, C., Fassbender, A. J., Feely, R. A., González-Dávila, M., Goyet, C., Hales, B., Hardman-Mountford, N., Heinze, C., Hood, M.,

BGD

doi:10.5194/bg-2015-606

Hoppema, M., Hunt, C. W., Hydes, D., Ishii, M., Johannessen, T., Jones, S. D., Key, R. M., Körtzinger, A., Landschützer, P., Lauvset, S. K., Lefèvre, N., Lenton, A., Lourantou, A., Merlivat, L., Midorikawa, T., Mintrop, L., Miyazaki, C., Murata, A., Nakadate, A., Nakano, Y., Nakaoka, S., Nojiri, Y., Omar, A. M., Padin, X. A., Park, G.-H., Paterson, K., Perez, F. F., Pierrot, D., Poisson, A., Ríos, A. F., Santana-Casiano, J. M., Salisbury, J., Sarma, V. V. S. S., Schlitzer, R., Schneider, B., Schuster, U., Sieger, R., Skjelvan, I., Steinhoff, T., Suzuki, T., Takahashi, T., Tedesco, K., Telszewski, M., Thomas, H., Tilbrook, B., Tjiputra, J., Vandemark, D., Veness, T., Wanninkhof, R., Watson, A. J., Weiss, R., Wong, C. S., and Yoshikawa-Inoue, H.: A uniform, quality controlled Surface Ocean CO_2 Atlas (SOCAT), Earth Syst. Sci. Data, 5, 125–143, doi:10.5194/essd-5-125-2013, 2013.

Piontek, J., Händel, N., Langer, G., Wohlers, J., Riebesell, U., and Engel, A.: Effects of rising temperature on the formation and microbial degradation of marine diatom aggregates, Aquat. Microb. Ecol., 54, 305–318, doi:10.3354/ame01273, 2009.

Qiu, B. and Gao, K.: Effects of CO_2 enrichment on the bloom-forming cyanobacterium Microcystis aeruginosa (Cyanophyceae): physiological responses and relationships with the availability of dissolved inorganic carbon, J. Phycol., 38, 721–729, doi:10.1046/j.1529-8817.2002.01180.x, 2002.

Raven, J. A.: The twelfth Tansley Lecture. Small is beautiful: the picophytoplankton, Funct. Ecol., 12, 503–513, doi:10.1046/j.1365-2435.1998.00233.x, 1998.

Riebesell, U. and Tortell, P. D.: Effects of ocean acidification on pelagic organisms and ecosystems, in: Ocean Acidification, edited by: Gattuso, J. P. and Hansson, L., Oxford University Press, Oxford, UK, 99–121, 2011.

Riebesell, U., Körtzinger, A., and Oschlies, A.: Sensitivities of marine carbon fluxes to ocean change, P. Natl. Acad. Sci. USA, 106, 20602–20609, doi:10.1073/pnas.0813291106, 2009.

Riemann, L., Leitet, C., Pommier, T., Simu, K., Holmfeldt, K., Larsson, U., and Hagström, Å.: The native bacterioplankton community in the central Baltic Sea is influenced by freshwater bacterial species, Appl. Environ. Microb., 74, 503–515, doi:10.1128/AEM.01983-07, 2008.

Rose, J. M., Feng, Y., Gobler, C. J., Gutierrez, R., Harel, C. E., Leblancl, K., and Hutchins, D. A.: Effects of increased pCO_2 and temperature on the North Atlantic spring bloom, II. Microzooplankton abundance and grazing, Mar. Ecol.-Prog. Ser., 388, 27–40, doi:10.3354/meps08134, 2009.

BGD
doi:10.5194/bg-2015-606

Schaum, E., Rost, B., Millar, A. J., and Collins, S.: Variation in plastic responses of a globally distributed picoplankton species to ocean acidification, 3, 298–302, doi:10.1038/NCLIMATE1774, 2012.
Sheik, A. R., Brussaard, C. P. D., Lavik, G., Lam, P., Musat, N., Krupke, A., Littmann, S., Strous, M., and Kuypers, M. M. M.: Responses of the coastal bacterial community to viral infection of the algae Phaeocystis globosa, ISME J., 8, 212–25, doi:10.1038/ismej.2013.135, 2014.
Sherr, E. B., Caron, D. A., and Sherr, B. F.: Staining of heterotrophic protists for visualization via epifluorescence microscopy, in: Current Methods in Aquatic Microbial Ecology, edited by: Kemp, J. C. P., Sherr, B., and Sherr, E., Lewis Publ., New York, USA, 213–228, 1993.
Spilling, K., Paul, A. J., Virkkala, N., Hastings, T., Lischka, S., Stuhr, A., Bermudez, R., Czerny, J., Schulz, K G., Ludwig, A., and Riebesell, U.: Ocean acidification decreases plankton respiration: evidence from a mesocosm experiment, Biogeosciences, 2015.
Suffrian, K., Simonelli, P., Nejstgaard, J. C., Putzeys, S., Carotenuto, Y., and Antia, A. N.: Microzooplankton grazing and phytoplankton growth in marine mesocosms with increased CO_2 levels, Biogeosciences, 5, 1145–1156, doi:10.5194/bg-5-1145-2008, 2008.
Suttle, C. A.: Viruses in the sea, Nature, 437, 356–361, doi:10.1038/nature04160, 2005.
Tortell, P. D., DiTullio, G. R., Sigman, D. M., and Morel, F. M. M.: CO_2 effects on taxonomic composition and nutrient utilization in an Equatorial Pacific phytoplankton assemblage, Mar. Ecol.-Prog. Ser., 236, 37–43, 2002.
Traving, S. J., Clokie, M. R. J., and Middelboe, M.: Increased acidification has a profound effect on the interactions between the cyanobacterium Synechococcus sp. WH7803 and its viruses, FEMS Microbiol. Ecol., 87, 133–141, doi:10.1111/1574-6941.12199, 2014.
Turley, C. and Boot, K.: UNEP Emerging Issues: Environmental Consequences of Ocean Acidification: A Threat to Food Security, United Nations Environment Programme, 2010.
Veldhuis, M. J. W. and Kraay, G. W.: Phytoplankton in the subtropical Atlantic Ocean: towards a better assessment of biomass and composition, Deep.-Sea. Res. Pt. I, 51, 507–530, doi:10.1016/j.dsr.2003.12.002, 2004.
Veldhuis, M. J. W., Timmermans, K. R., Croot, P., and Van Der Wagt, B.: Picophytoplankton; A comparative study of their biochemical composition and photosynthetic properties, J. Sea Res., 53, 7–24, doi:10.1016/j.seares.2004.01.006, 2005.

BGD
doi:10.5194/bg-2015-606

Waterbury, J. B., Watson, S. W., Valois, F. W., and Franks, D. G.: Biological and ecological characterization of the marine unicellular cyanobacterium Synechococcus, in: Photosynthetic Picoplankton, edited by: Platt, E. T. and Li, W., Can. Bull. Fish. Aquat. Sci., 214, 71–120, 1986.
Weinbauer, M. G.: Ecology of prokaryotic viruses, FEMS Microbiol. Rev., 28, 127–181, doi:10.1016/j.femsre.2003.08.001, 2004.
Weinbauer, M. G. and Suttle, C. A.: Potential significance of lysogeny to bacteriophage production and bacterial mortality in coastal waters of the Gulf of Mexico, Appl. Environ. Microb., 62, 4374–4380, 1996.
Weinbauer, M. G., Mari, X., and Gattuso, J.-P.: Effect of ocean acidification on the diversity and activity of heterotrophic marine microorganisms, in: Ocean Acidification, edited by: Gattuso, J. P. and Hansson, L., Oxford University Press, Oxford, UK, 83–98, 2011.
Wilhelm, S. W. and Suttle, C. A.: Viruses and nutrient cycles in the Sea aquatic food webs, Bioscience, 49, 781–788, doi:10.2307/1313569, 1999.
Wilhelm, S. W., Brigden, S. M., and Suttle, C. A.: A dilution technique for the direct measurement of viral production: a comparison in stratified and tidally mixed coastal waters, Microb. Ecol., 43, 168–173, doi:10.1007/s00248-001-1021-9, 2002.
Winget, D. M., Williamson, K. E., Helton, R. R., and Wommack, K. E.: Tangential flow diafiltration: an improved technique for estimation of virioplankton production, Aquat. Microb. Ecol., 41, 221–232, doi:10.3354/ame041221, 2005.
Wohlers, J., Engel, A., Zöllner, E., Breithaupt, P., Jürgens, K., Hoppe, H.-G., Sommer, U., and Riebesell, U.: Changes in biogenic carbon flow in response to sea surface warming, P. Natl. Acad. Sci. USA, 106, 7067–7072, doi:10.1073/pnas.0812743106, 2009.
Wohlers-Zöllner, J., Breithaupt, P., Walther, K., Jürgens, K., and Riebesell, U.: Temperature and nutrient stoichiometry interactively modulate organic matter cycling in a pelagic algal-bacterial community, Limnol. Oceanogr., 56, 599–610, doi:10.4319/lo.2011.56.2.0599, 2011.
Wolf-Gladrow, D. and Riebesell, U.: Diffusion and reactions in the vicinity of plankton: a refined model for inorganic carbon transport, Mar. Chem., 59, 17–34, doi:10.1016/S0304-4203(97)00069-8, 1997.
Zondervan, I., Rost, B., and Riebesell, U.: Effect of CO_2 concentration on the PIC/POC ratio in the coccolithophore Emiliania huxleyi grown under light-limiting conditions and different daylengths, J. Exp. Mar. Bio. Ecol., 272, 55–70, doi:10.1016/S0022-0981(02)00037-0, 2002.

BGD
doi:10.5194/bg-2015-606

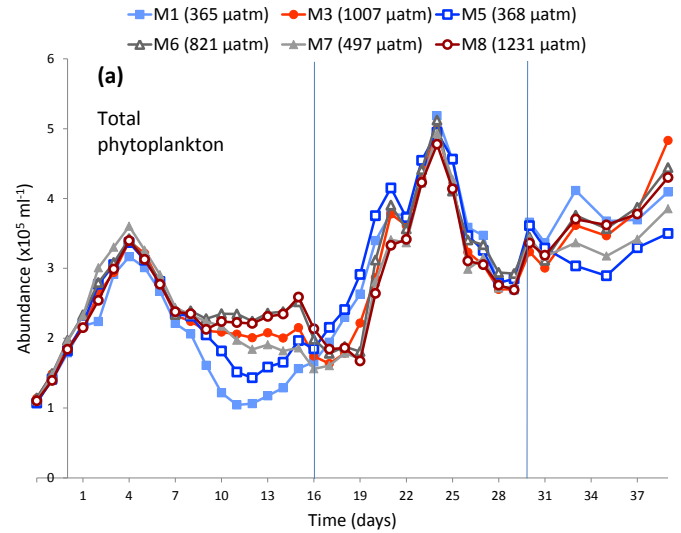

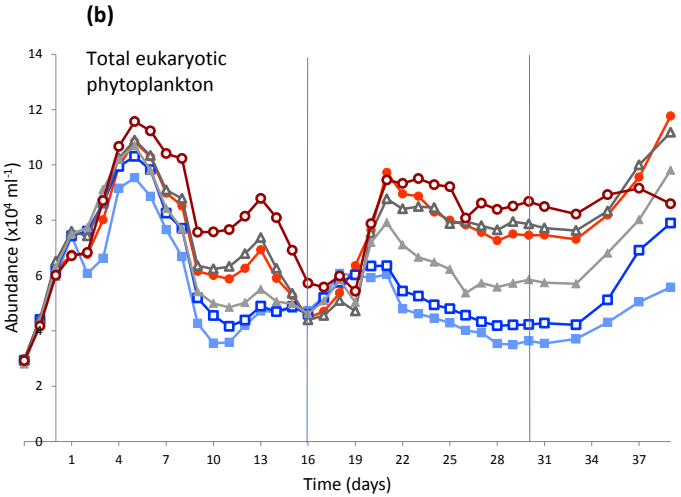

BGD
doi:10.5194/bg-2015-606

Shifts in the microbial community in the Baltic Sea with increasing CO_2

K. J. Crawfurd et al.

Figure 1. (a) Temporal dynamics of depth-integrated upper layer (0.3–10 m) total phytoplankton and **(b)** total eukaryotic phytoplankton, i.e. all except the prokaryotic photoautotroph *Synechococcus* spp. Lines indicate the start and end of phase II. The colours and symbols used in the legend are consistent throughout subsequent figures and, in parenthesis, is shown the mean fCO_2 across the duration of the experiment i.e. days 1–43.

BGD
doi:10.5194/bg-2015-606

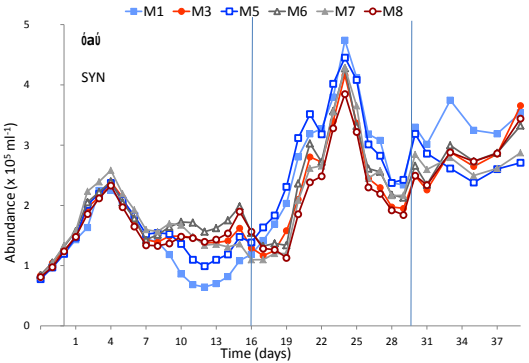

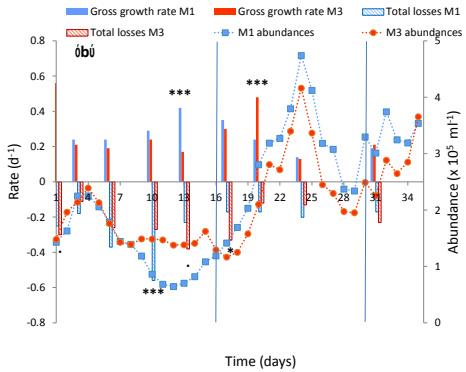

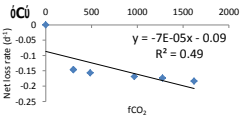

BGD
doi:10.5194/bg-2015-606

Shifts in the microbial community in the Baltic Sea with increasing CO_2

K. J. Crawfurd et al.

Figure 2. (a) Temporal dynamics of depth-integrated upper layer (0.3–10 m) total prokaryotic phytoplankton, *Synechococcus* spp., whereby the lines indicate the different phases (I–III). **(b)** Abundances for mesocosm M1 (control, blue line) and mesocosm M3 (high CO_2, red line), with gross growth displayed as bars above the x axis and total losses as bars below the x axis. A failed experiment is indicated by f, otherwise no data is a zero. Significant differences between mesocosms are marked: *** $p \leq 0.001$, ** $p \leq 0.01$, * $p \leq 0.05$, $p \leq 0.1$. **(c)** Specific growth rates derived from exponential regression of the net SYN abundances, versus average fCO_2 for days 4–7.

BGD
doi:10.5194/bg-2015-606

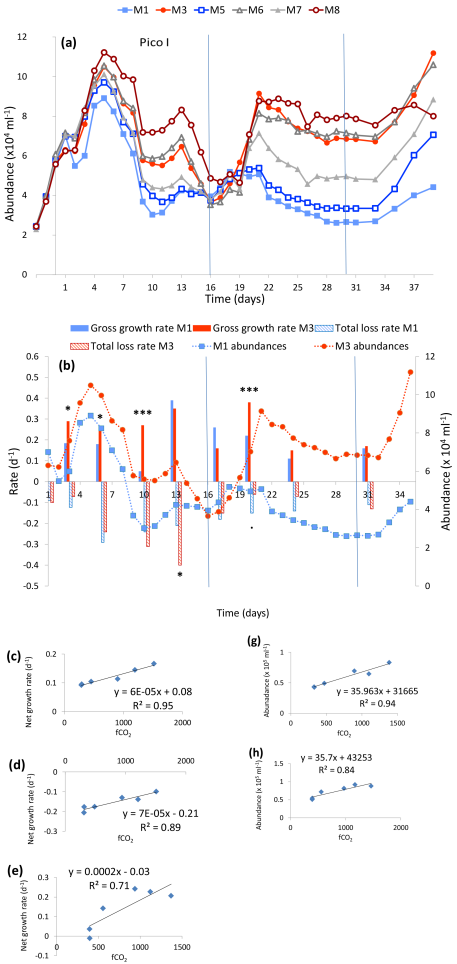

BGD
doi:10.5194/bg-2015-606

Shifts in the microbial community in the Baltic Sea with increasing CO_2

K. J. Crawfurd et al.

Figure 3. (a) Temporal dynamics of depth-integrated upper layer (0.3–10 m) picophytoplankton I (Pico I). **(b)** Abundances for mesocosm M1 (control, blue line) and mesocosm M3 (high CO_2, red line), with gross growth displayed as bars above the x axis and total losses as bars below the x axis. A failed experiment is indicated by f, otherwise no data is a zero. Significant differences between mesocosms are marked: $p \leq 0.001^{***}$, $p \leq 0.01^{**}$, $p \leq 0.05^{*}$, $p \leq 0.1$. **(c)** Specific growth rates derived from exponential regression of the net Pico I abundances, vs. average fCO_2 for days 1–5; **(d)** days 5–9; **(e)** days 18–21, a negative growth rate indicates cell loss. **(f)** Phytoplankton cell abundance vs. actual fCO_2 for Pico I on days 5; **(g)** 13 **(h)** 21. Linear regression statistics provided in plots.

BGD
doi:10.5194/bg-2015-606

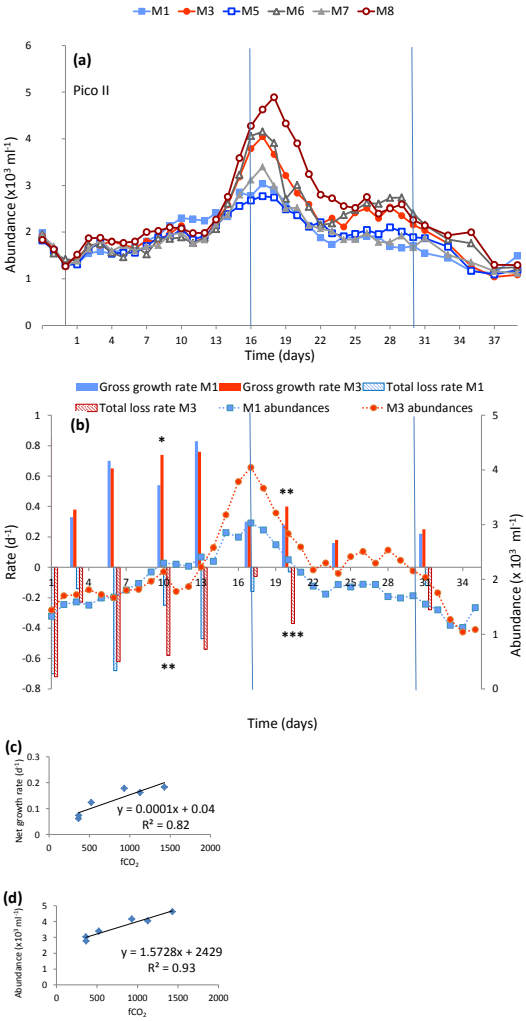

BGD
doi:10.5194/bg-2015-606

Shifts in the microbial community in the Baltic Sea with increasing CO_2

K. J. Crawfurd et al.

Figure 4. (a) Temporal dynamics of depth-integrated upper layer (0.3–10 m) picoeukaryotic phytoplankton II (Pico II). **(b)** Abundances for mesocosm M1 (control, blue line) and mesocosm M3 (high CO_2, red line), with gross growth displayed as bars above the x axis and total losses as bars below the x axis. A failed experiment is indicated by f, otherwise no data is a zero. Significant differences between mesocosms are marked: $p \leq 0.001^{***}$, $p \leq 0.01^{**}$, $p \leq 0.05^{*}$, $p \leq 0.1$. **(c)** Specific growth rate determined from the net Pico II abundances, vs. average fCO_2 for days 12–17. **(d)** Phytoplankton cell abundance vs. actual fCO_2 for Pico I on day 17. Linear regression statistics provided in plots.

BGD
doi:10.5194/bg-2015-606

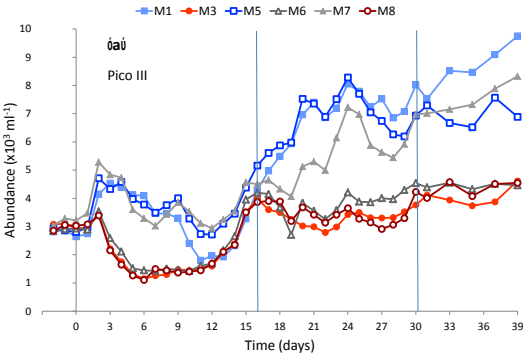

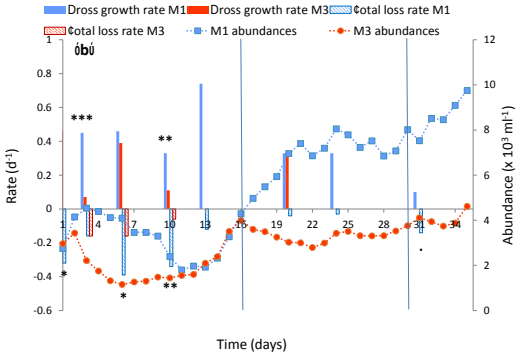

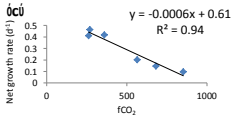

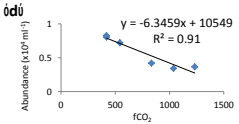

BGD
doi:10.5194/bg-2015-606

Shifts in the microbial community in the Baltic Sea with increasing CO_2

K. J. Crawfurd et al.

Figure 5. (a) Temporal dynamics of depth-integrated upper layer (0.3–10 m) picoeukaryotic phytoplankton III (Pico III). **(b)** Abundances for mesocosm M1 (control, blue line) and mesocosm M3 (high CO_2, red line), with gross growth displayed as bars above the x axis and total losses as bars below the x axis. A failed experiment is indicated by f, otherwise no data is a zero. Significant differences between mesocosms are marked: $p \leq 0.001^{***}$, $p \leq 0.01^{**}$, $p \leq 0.05^{*}$, $p \leq 0.1$. **(c)** Specific growth rate determined from the net Pico III abundances, vs. average fCO_2 for days 1–2. **(d)** Phytoplankton cell abundance vs. actual fCO_2 for Pico I on day 24. Linear regression statistics provided in plots.

BGD
doi:10.5194/bg-2015-606

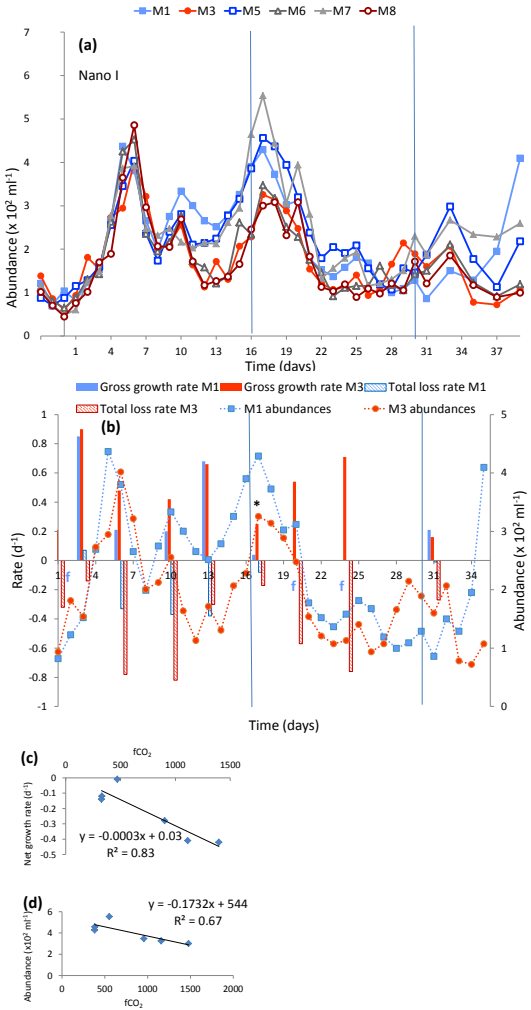

BGD
doi:10.5194/bg-2015-606

Shifts in the microbial community in the Baltic Sea with increasing CO_2

K. J. Crawfurd et al.

Figure 6. (a) Temporal dynamics of depth-integrated upper layer (0.3–10 m) nanoeukaryotic phytoplankton I (Nano I). **(b)** Abundances for mesocosm M1 (control, blue line) and mesocosm M3 (high CO_2, red line), with gross growth displayed as bars above the x axis and total losses as bars below the x axis. A failed experiment is indicated by f, otherwise no data is a zero. Significant differences between mesocosms are marked: $p \leq 0.001^{***}$, $p \leq 0.01^{**}$, $p \leq 0.05^{*}$, $p \leq 0.1$. **(c)** Specific growth rate determined from the net Nano I abundances, vs. average fCO_2 for days 10–12, a negative growth rate indicates cell loss **(d)** Phytoplankton cell abundance vs. actual fCO_2 for Nano I on day 17. Linear regression statistics provided in plots.

BGD
doi:10.5194/bg-2015-606

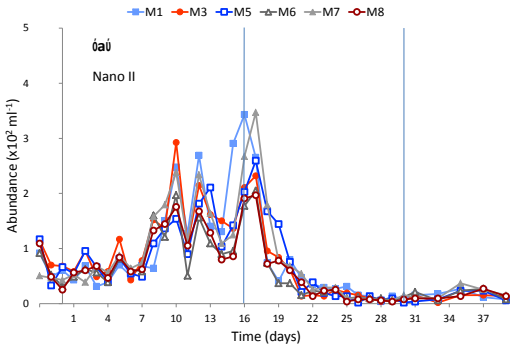

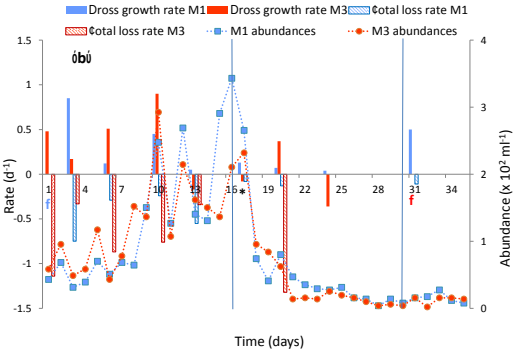

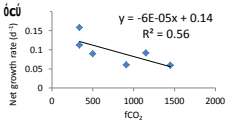

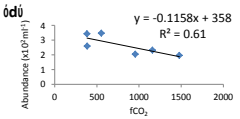

BGD
doi:10.5194/bg-2015-606

Shifts in the microbial community in the Baltic Sea with increasing CO_2

K. J. Crawfurd et al.

Figure 7. (a) Temporal dynamics of depth-integrated upper layer (0.3–10 m) nanoeukaryotic phytoplankton II (Nano II). **(b)** Abundances for mesocosm M1 (control, blue line) and mesocosm M3 (high CO_2, red line), with gross growth displayed as bars above the x axis and total losses as bars below the x axis. A failed experiment is indicated by f, otherwise no data is a zero. Significant differences between mesocosms are marked: $p \leq 0.001^{***}$, $p \leq 0.01^{**}$, $p \leq 0.05^{*}$, $p \leq 0.1$. **(c)** Specific growth rate determined from the net Nano II abundances, vs. average fCO_2 for days 6–17 (M1, days 6–16) **(d)** Phytoplankton cell abundance vs. actual fCO_2 for Nano II on day 17 (M1, day 16). Linear regression statistics provided in plots.

BGD
doi:10.5194/bg-2015-606

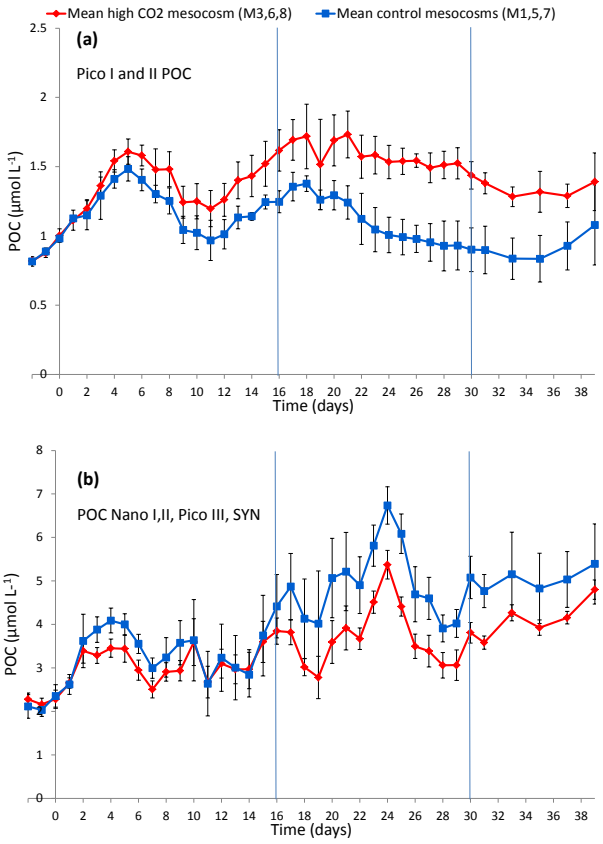

Figure 8. POC calculated from mean cell abundances assuming cells to be spherical and to contain 0.2 pg C μm^{-3} (Waterbury et al., 1986), error bars show one standard deviation. **(a)** Temporal dynamics of Pico I and II **(b)** Temporal dynamics of POC for all other groups i.e. SYN, Pico III, Nano I and II.

BGD
doi:10.5194/bg-2015-606

Shifts in the microbial community in the Baltic Sea with increasing CO_2

K. J. Crawfurd et al.

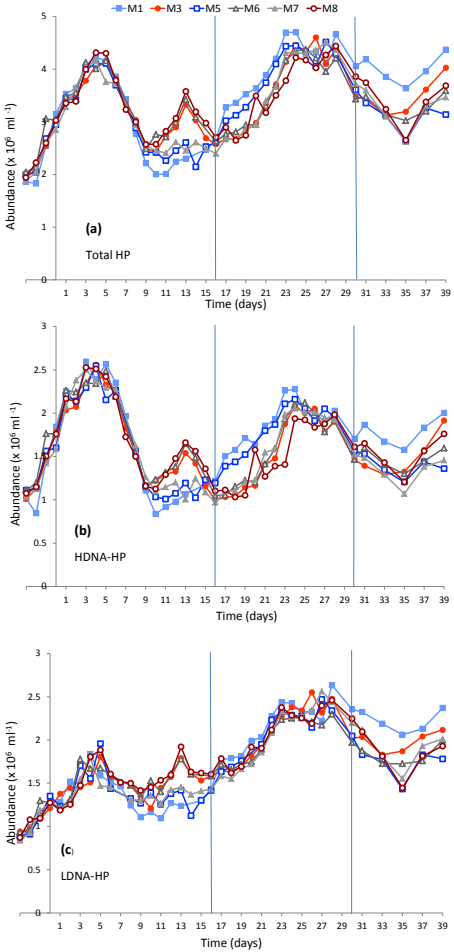

BGD
doi:10.5194/bg-2015-606

Shifts in the microbial community in the Baltic Sea with increasing CO_2

K. J. Crawfurd et al.

Figure 9. (a) Temporal dynamics of depth-integrated upper layer (0.3–10 m) total heterotrophic prokaryotes (HP) **(b)** High DNA fluorescence heterotrophic prokaryotes (HDNA-HP) **(c)** Low DNA fluorescence heterotrophic prokaryotes (LDNA-HP).

BGD
doi:10.5194/bg-2015-606

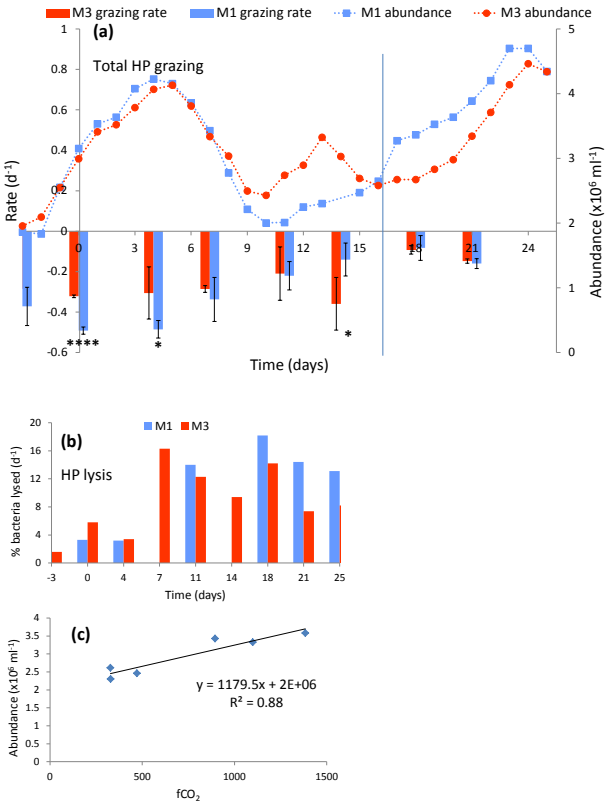

Figure 10. (a) M1 (control) and M3 (high CO_2) temporal dynamics of total heterotrophic prokaryotes (HP), abundances and grazing rates (d^{-1}) (bars below the *x* axis). **(b)** Viral lysis as percentage of HP standing stock in mescocosm M1 (low fCO_2, blue line) and M3 (high fCO_2, red line), **(c)** Total HP cell abundance vs. actual fCO_2 on day 13. Linear regression statistics provided in plots. Significant differences between mesocosms are marked: $p \leq 0.001^{***}$, $p \leq 0.01^{**}$, $p \leq 0.05^{*}$, $p \leq 0.1$.

BGD
doi:10.5194/bg-2015-606

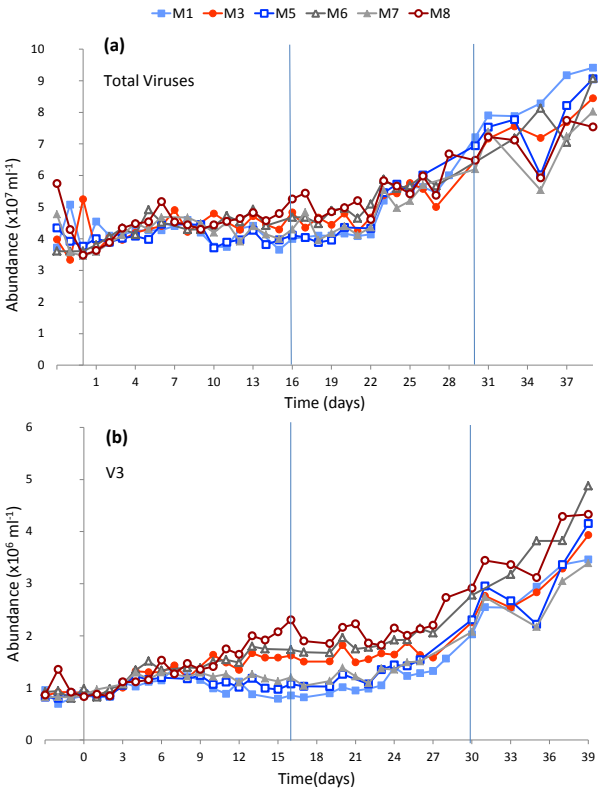

Figure 11. (a) Temporal dynamics of depth-integrated upper layer (0.3–10 m) total virus abundances, **(b)** Virus group V3, discriminated by its higher green nucleic acid-specific fluorescence.

BGD
doi:10.5194/bg-2015-606

Shifts in the microbial community in the Baltic Sea with increasing CO_2

K. J. Crawfurd et al.